Transcranial FUS-Evoked Functional Ultrasound Imaging in Non-Human Primates

Saachi Munot[1], Samuel Blackman[1], Anthony Mathai[2], Fotios Tsitsos[1], Elisa Konofagou[1,3,4]
[1]*Department of Biomedical Engineering, Columbia University, New York, NY, USA*
[2]*Department of Biomedical Engineering, City College of New York, New York NY, USA*
[3]*Department of Radiology, Columbia University, New York, NY, USA*
[4]*Department of Neurological Surgery, Columbia University, New York, NY, USA*
Email: spm2195@columbia.edu

2025 IEEE International Ultrasonics Symposium (IUS) | 979-8-3315-2332-9/25/$31.00 ©2025 IEEE | DOI: 10.1109/IUS62464.2025.11201742

***Abstract*- We demonstrate fully transcranial functional ultrasound imaging (fUSI) and, to our knowledge, the first transcranial readout of focused ultrasound (FUS)-evoked hemodynamics through the intact primate skull using a confocally aligned, coaxial stimulation–imaging assembly in an adult cynomolgus macaque. Ultrafast Doppler acquisitions (800-frame ensembles at 800 Hz PRF) were interleaved with 0.5-MHz FUS pulse trains (250-ms, amplitude-modulated bursts at 0.75 Hz), and activation was mapped via HRF-based correlation with Bonferroni correction and overlaid on vascular ground truth from contrast-enhanced Power Doppler (CEPD) and ultrasound localization microscopy (ULM). FUS produced spatially localized increases in cerebral blood volume centered on the acoustic focus with onset ~5-10 s after stimulus onset and return toward baseline after stimulus offset; positively and negatively correlated compartments followed vessel-like trajectories and co-registered with CEPD/ULM vasculature. Across a pressure sweep (estimated derated peak positive pressure ~0.97, 1.40, 1.81 MPa), activation magnitude, spatial extent, and correlation strength increased (Bonferroni-corrected activated kernels ~1,782 to 2,94 to 4,682; ROI peak responses up to ~7.5% ΔCBV), while extending the train length (5/10/20/30 pulses) further increased area-under-the-curve and peak amplitude (up to ~8.2% ΔCBV) without markedly shifting onset latency. These results establish transcranial fUSI as a practical on-target readout for ultrasound neuromodulation - enabling targeting, dose–response quantification, and mechanistic assessment - and outline a path toward image-guided, human-relevant protocols.**

***Keywords* - Focused ultrasound (FUS), functional ultrasound (fUSI), Neurovascular Response, Transcranial, NHP.**

I. INTRODUCTION

Functional ultrasound imaging (fUSI) is a neuroimaging tool that leverages ultrafast Doppler to read out neurovascular dynamics with high spatiotemporal resolution [1]. Foundational studies in small animals have demonstrated robust stimulus-evoked [2] and spontaneous network mapping [3], and early translational work has shown feasibility in primates [4, 5] and humans [6, 7] when an acoustic window is available. However, translation to fully transcranial applications in primates - including humans - has been limited by the thicker, more heterogeneous skull, which introduces strong attenuation, phase aberrations, and reverberation noise, degrading sensitivity and spatial fidelity [8]. Consequently, fully transcranial fUSI in primates has, to date, proved difficult. Meanwhile, focused ultrasound stimulation (FUS) has emerged as a promising noninvasive technique for modulating brain activity and the neurovascular unit across rodent and primate models. Relative to transcranial magnetic or electrical stimulation, FUS offers higher spatial specificity and access to deeper targets. Outside MRI environments, however, practical, real-time methods for target verification and on-target dose–response quantification remain limited. Separately, in situ functional readouts are needed to verify neurovascular engagement and elucidate mechanisms such as distinguishing acute vs durable effects, excitation vs suppression, and parameter-dependent pathways. Studies have examined FUS-evoked hemodynamic responses in mice under both craniotomized [9] and intact-skull preparations [10], but translation to thicker-skulled animal models has remained limited.

The objectives of this study are to use a coaxial stimulation-imaging assembly to demonstrate (1) fully transcranial fUSI in non-human primates and quantify FUS-evoked hemodynamics through the intact skull; (2) dose-response characterization across acoustic pressure and stimulus duration using HRF-based activation metrics; and (3) spatial validation via registration of activation maps to vasculature with contrast-enhanced Power Doppler and ultrasound localization microscopy, including separation of positively and negatively correlated compartments.

II. METHODS

A. Non-Human Primate Preperation

An adult male cynomolgus macaque (Macaca fascicularis; ~140 months, ≈11.7 years) was sedated, intubated, and maintained under general anesthesia. An intravenous catheter was placed in the saphenous vein for administration of fluids and microbubbles. The head was immobilized in a stereotactic frame using a custom bite block. Anesthesia was continuously monitored by on-site veterinary staff throughout the procedure. The hair on the scalp was clipped and any residual hair was removed with a commercial depilatory cream (Nair) to ensure reliable acoustic coupling. Respiratory rate, heart rate, and oxygen saturation (SpO_2) were continuously monitored. All procedures were approved by the Columbia University Institutional Animal Care and Use Committee (IACUC).

B. Neuronavigation-Based Targeting and k-Wave Simulations

Target regions were chosen in functionally meaningful cortical regions (prefrontal and sensorimotor cortex), prioritizing beam paths that minimized skull incidence angle and avoided thick temporalis muscle. Specific targets and beam trajectories were chosen by optimizing simulated transmission and derated peak negative pressure at the focal zone. Forward acoustic simulations were performed in k-Wave (MATLAB) for the H204 (focused transducer described in section C) emitting at 0.5 MHz. For in-vivo guidance, we used optical neuronavigation (Brainsight; Rogue Research, Montreal, QC, Canada). The animal's head and the transducer were registered to the anatomical volume and planned target and entry points from the simulation plan were imported into Brainsight. The transducer pose was aligned to the planned beam axis using tracked fiducials and continuously visualized relative to the target and skull surface. Position and orientation were maintained within system tolerance during sonication.

C. Focused Ultrasound Stimulation

A single-element spherical FUS transducer (carrier 0.5 MHz; H-204, Sonic Concepts Inc, Bothell, WA) with a focal size of ~0.5x2 cm was confocally aligned with the ultrasound imaging array via a coaxial mount, sharing a single acoustic opening. The transducer was coupled to the scalp through a sealed water-bath chamber (acoustically transparent membrane) filled with deionized, degassed water. The FUS drive chain comprised a function generator feeding an RF power amplifier connected to the transducer. During FUS blocks, the imaging system triggered the function generator immediately after each image acquisition to avoid interference between FUS and fUSI. Amplitude-modulated pulses of 250 ms at 0.5 MHz, delivered at a 0.75 Hz PRF were interleaved with imaging pulses. Both the estimated derated peak positive pressure assuming 60% attenuation (~0.97-1.81 MPa) and number of stimulation pulses (5, 10, 20, 30) were varied across trials. Each stimulation block consisted of 15-30s pre-stimulation baseline, FUS, and a 15-30s post-stimulation baseline; blocks were repeated within each session, and at least three trials per condition were averaged.

D. Functional Ultrasound Imaging and Analysis

A broadband ultrasound imaging array (P4-2, ATL/Philips, Andover, MA, USA) was coaxially aligned and confocal with the FUS transducer. Ultrafast Doppler acquisitions were run in an interleaved, non-overlapping sequence with stimulation: for each block, high-frame-rate Doppler ensembles of 800 frames (pulse-repetition frequency of 800 Hz) were acquired on a ~0.75 Hz cycle to generate Power Doppler (PD) images. Post processing (beamforming, clutter suppression, PD integration) produced time-resolved PD volumes. %ΔCBV (cerebral blood volume) was computed by normalizing Power Doppler to the 15-30 s pre-stimulation baseline. For activation mapping, the stimulus design was convolved with a canonical hemodynamic response function (HRF) to create the HRF regressor. This was then cross correlated with the %ΔCBV time series for λ/2-sized kernels. Resulting correlation maps were thresholded with a Bonferroni correction across image pixels to control family-wise error. For visualization, median-filtered thresholded activation maps were overlaid on contrast-enhanced Power Doppler (CEPD) images. Trial-averaged CBV traces were extracted from vascular regions of interest (ROIs), and summary metrics, peak %ΔCBV, peak duration, and area under the curve (AUC), were computed per condition.

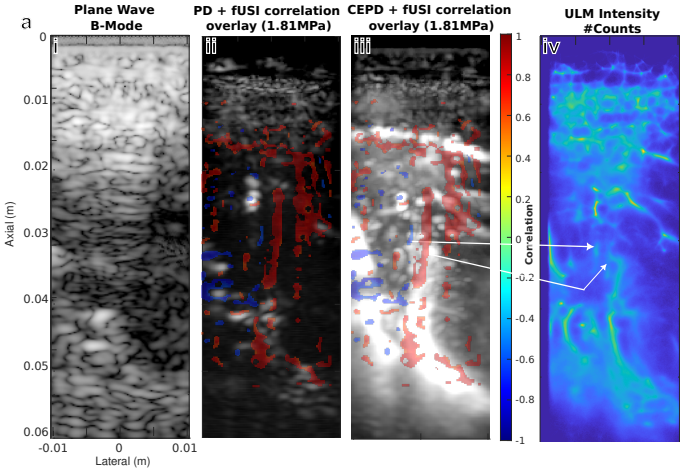

Figure 1: Ultrasound Imaging Pipeline and FUS-evoked fUSI correlation maps of NHP brain (red = postively, blue = negatively correlated) i) Transcranial Plane wave B-Mode image of brain. ii) Contrast-free PD image overlayed with fUSI correlation maps (estimated derated peak positive pressure ~1.81 MPa). iii) Constrast Enhanced PD MIP overlayed with fUSI correlation maps. iv) ULM intensity map. Arrows from CEPD MIP to ULM intensity show resolved vascular compartments.

E. Contrast-Enhanced Power Doppler and Ultrasound Localization Microscopy

In order to establish a vascular ground truth for our fUSI correlation maps, we acquired contrast enhanced Power Doppler (CEPD) and ultrasound localization microscopy (ULM) at the same location used for stimulation and imaging. We used in-house, lipid-shelled microbubbles synthesized per our previously published protocol [11]. The microbubble concentration for the 1-10 μm diameter range was ~10^9 MB/mL (pre-dilution). Before imaging the bubbles were diluted by 1:10, 1:20, or 1:50 in saline to tune persistence for CEPD and sparsity for ULM. After the FUS-fUSI acquisitions, microbubbles were administered and ultrafast Doppler data was acquired. For each CEPD/ULM block, we acquired 500-800 frames at a ~800 Hz PRF from the same transducer placement. The same raw dataset was processed in two ways: (i) CEPD, via clutter-suppressed integration of post-contrast Power Doppler to visualize and register vasculature; and (ii) ULM intensity and velocity maps, processed with our ULM pipeline to generate super-resolution vascular maps and flow estimates. The resulting CEPD Maximum Intensity Projections (MIP) across blocks and ULM maps were co-registered with the fUSI data and used to interpret spatial patterns and delineate positively vs negatively correlated compartments, validate the vascular substrate of activations, and guide ROI definition.

III. RESULTS

A. FUS stimulation evokes localized CBV increases

Transcranial FUS produced spatially localized hemodynamic responses centered on and around the acoustic

focus. Bonferroni-corrected HRF correlation maps showed compact clusters of positively correlated pixels (red) with negatively correlated regions (blue) in adjacent vasculature (Fig 1, ii, iii, iv). For the 1.81 MPa, 20 frames case, ROI-averaged %ΔCBV traces (Fig. 1, iii; Fig. 2, b. iii) rose during the stimulation epoch first peaks at ~ 5-10 seconds (4-8 frames) relative to onset and returned toward baseline around 10-20s post offset. Peak amplitudes reached up to ~7.5 %ΔCBV in the most responsive ROI, with response width and AUC increasing with stimulus dose - increasing pressure and stimulation duration (Fig.2, 3). Spatially, the activation was clustered in a column like structure around the assumed focus. Positive clusters tracked vessel-like trajectories within the parenchyma, whereas smaller negative patches appeared in neighboring compartments. Overlays on CEPD sharpened this correspondence, and the ULM intensity map reproduced the same vascular geometry underlying the red/blue pattern (Fig. 1, ii–iv).

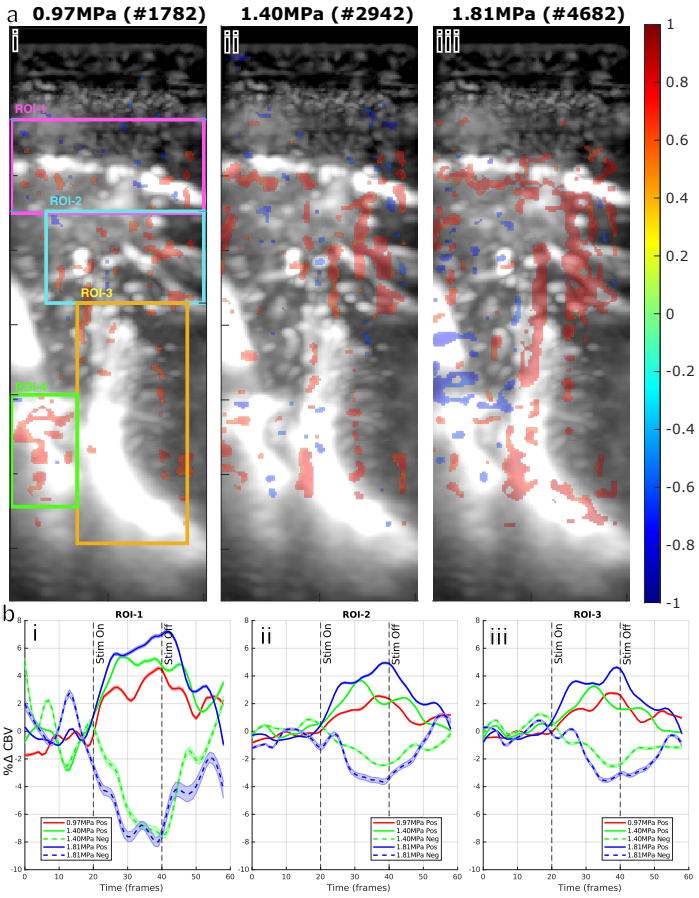

Figure 2: a. FUS-evoked fUSI correlation maps with increasing FUS pressure overlayed on CEPD MIP. a.i-iii) FUS pressures of ~0.97 MPa, ~1.40 MPa, ~1.81 MPa (60% attenuation) with 1782, 2942 and 4682 activated λ/4-sized kernels. b. i-iii) %Δ CBV traces per pressure averaged over trials and ROIs (blue is ~1.81 MPa, green is ~1.40 MPa, red is ~0.97 MPa) over 60 frames. Solid lines are for positively correlated pixels, dashed lines are for negatively correlated pixels. Standard deviation across kernels and trials envelope each trace. Each column i-iii represents a regions of interest overlayed in a.i. Note traces only plotted for ROIs with greater than 25 correlated kernels.

B. CBV increases scale with FUS pressure

To characterize the pressure dependence of the hemodynamic response we increased the derated acoustic pressure from 0.97 MPa to 1.40 MPa to 1.81 MPa. The FUS-evoked neurovascular response increased in magnitude, spatial extent and correlation strength of activation (Fig 2). The number of correlated pixels (after Bonferroni correction) rose from 1,782 to 2,942 to 4,682 (Fig. 2, 4). Correspondingly, we also see an increase in %ΔCBV peaks (Fig 2.b). For example, in ROI1 this increases from a 5% to 7% as the estimated derrated pressure increases from 1.40 MPa to 1.81 MPa. Similarly, we also see an increase in the area under the curve. Moreover, the spatial topology was preserved with increased pressure. Higher pressure yielded a concentric expansion around the same columnar region, with incremental recruitment at the periphery and stronger correlations within the core.

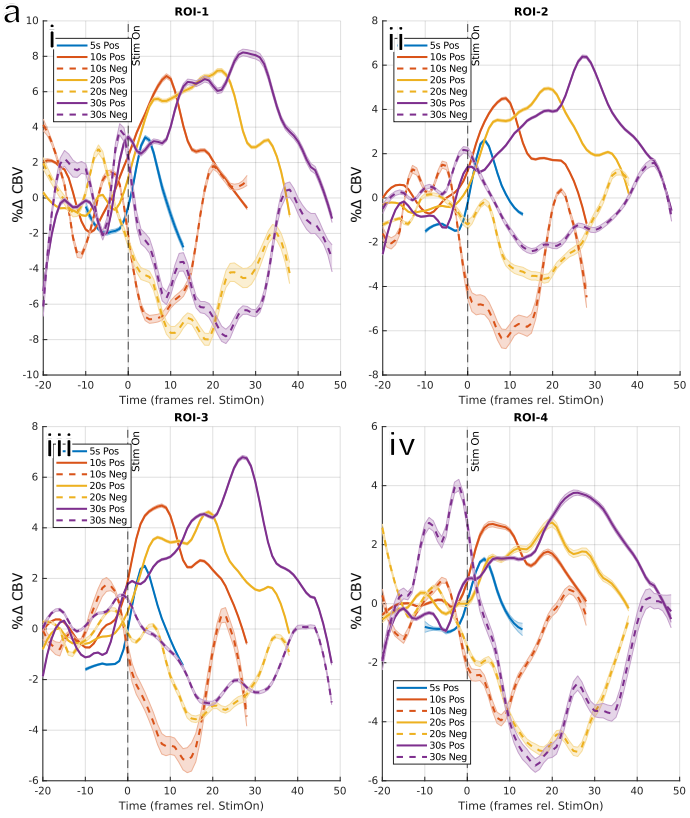

Figure 3: i-iv - FUS-evoked %ΔCBV traces averaged over trials and ROIs, for different stimulation durations - 5, 10, 20, 30 pulses respectively (represented by different colors in the plot). Frame 0 is the stimulus start for all stimulus durations. Solid lines are for positively correlated pixels; dashed lines are for negatively correlated pixels. Standard deviation across kernels and trials envelope each trace. Each column i-iii represents a regions of interest overlayed in a.i. Note traces only plotted for ROIs with greater than 25 correlated kernels.

C. CBV increases scale with stimulus-train duration

To further understand the dose-dependence of our neurovascular response and its temporal characteristics we varied the stimulation duration of our FUS pulses at a given pressure (~1.81 MPa) to 5, 10, 20 and 30 pulses. Increasing the train length (5, 10, 20, 30 pulses) produced larger and more sustained responses (Fig. 3, i-iv). AUC and peak duration increased roughly monotonically with duration, and peak %ΔCBV reached up to ~8.2% at 30 s. In all ROIs, the onset latency was comparatively stable across pulse durations. The the traces began to rise ~5-10 s (≈4-8 frames) after S*tim*

On, indicating that onset timing is governed primarily by vascular transit and dilation. With longer trains, the waveform exhibited a maintained elevation during stimulation and a peak before *Stim Off*, followed by a gradual return toward baseline; correspondingly, recovery time increased with duration, indicating that longer input broadens the hemodynamic response rather than substantially shifting its initial latency. Negative-correlation traces displayed complementary decreases with similar timing (Fig. 3, i–iv).

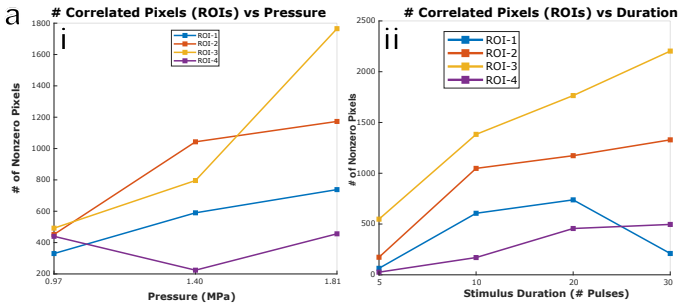

Figure 4: Number of Bonferroni-corrected correlated λ/4-sized kernels per ROI plotted against increasing (i) pressure and (ii) stim duration. Each color represents a ROI from 2.a.i (blue is ROI 1, red is ROI 2, yellow is ROI 3 and purple is ROI 4).

D. ROI-resolved hemodynamic profiles across dose

Using CEPD/ULM overlays, we defined four vascular ROIs (Fig 2. a.i) and compared %ΔCBV across pressure (0.97,1.40,1.81 MPa) and duration (5,10,20,30 frames) sweeps (Fig. 2a; Fig. 4). Across ROIs the temporal waveform was conserved: traces exhibited a brief latency after *Stim On*, and a gradual return toward baseline; with longer trains the response broadened while onset timing remained relatively unchanged. Dose primarily acted as gain (pressure) and gain + broadening (duration), while ROI-specific variability appeared as slight shifts in peak time and decay rate. Pixel-count curves emphasized these differences: with pressure (Fig. 3.i) ROI-1 increased sharply from ≈220 to ≈2,330 and then decreased to ≈770; ROI-2 rose from ≈460 to ≈1,200 to ≈2,240; ROI-3 rose from ≈470 to ≈1,030 to ≈2,240; ROI-4 peaked near 1.40 MPa at ≈1,030 and fell to ≈320. With duration (Fig. 4 ii), ROI-3 showed near-linear growth (~550 to ~2250), ROI-2 increased then plateaued (~120 to ~1300), ROI-4 rose steadily (~50 to ~480), and ROI-1 was non-monotonic, increasing to ~750 at 20s and decreasing by 30s (~200). Taken together, ROIs share a common HRF-like shape but differ slightly in dose–response slope and spatial distribution, consistent with regional vascular architecture and compartmental contributions.

IV. CONCLUSION

We have hereby demonstrate, the first, to our knowledge, fully transcranial functional ultrasound imaging in non-human primates and the first transcranial readout of FUS-evoked hemodynamics through an intact primate skull. Using a coaxial stimulation–imaging setup at 0.5 MHz, FUS produced spatially localized CBV increases at and around the focus that were dose-dependent: as acoustic pressure increased (≈0.97 to 1.81 MPa), the number of activated pixels rose (≈1,782 to 4,682), and ROI peaks reached up to ~7.5% ΔCBV; extending the pulse-train duration (5/10/20/30 s) further increased response magnitude and AUC (up to ~8.2% ΔCBV). Independently of stimulation, we also demonstrate transcranial fUSI imaging itself - contrast-enhanced Power Doppler and ULM acquired at the same placement - providing vascular ground truth that co-localizes positive/negative correlations to distinct compartments and supports ROI-resolved quantification. These findings are consistent with prior small-animal reports of FUS-evoked, dose-dependent neurovascular responses measured with fUSI, and they extend that evidence to a thicker-skulled primate model without craniotomy. Together, they establish transcranial fUSI as a practical readout for targeting, verification, and mechanistic assessment in ultrasound neuromodulation and outline a clear path toward image-guided, human-relevant protocols.

V. ACKNOWLEDGMENTS

This study was supported by National Institutes of Health (R01EB027576). SM was partly funded by the Blavatnik Foundation. The authors are grateful to Pablo Abreu, MA, for his administrative assistance. The authors also thank Seongyeon Kim, MS, Erica Paige McCune, MS, and Jonas Bendig, MD for their insightful discussions.

VI. REFERENCES

[1] G. Montaldo, A. Urban, and E. Macé, "*Annual Review of Neuroscience*, vol. 45, pp. 491–513, Jul. 2022, doi: https://doi.org/10.1146/annurev-neuro-111020-100706."

[2] E. Macé, G. Montaldo, I. Cohen, M. Baulac, M. Fink, and M. Tanter, "*Nature Methods*, vol. 8, no. 8, pp. 662–664, Aug. 2011, doi: https://doi.org/10.1038/nmeth.1641."

[3] B.-F. Osmanski, S. Pezet, A. Ricobaraza, Z. Lenkei, and M. Tanter, "*Nature Communications*, vol. 5, art. 5023, Oct. 2014, doi: https://doi.org/10.1038/ncomms6023."

[4] K. Blaize, F. Arcizet, M. Gesnik, H. Ahnine, U. Ferrari, T. Deffieux, P. Pouget, F. Chavane, M. Fink, J.-A. Sahel, M. Tanter, and S. Picaud, "*Proceedings of the National Academy of Sciences of the United States of America*, vol. 117, no. 25, pp. 14453–14463, Jun. 2020, doi: https://doi.org/10.1073/pnas.1916787117."

[5] A. Dizeux, M. Gesnik, H. Ahnine, K. Blaize, F. Arcizet, S. Picaud, J.-A. Sahel, T. Deffieux, P. Pouget, and M. Tanter, "*Nature Communications*, vol. 10, art. 1400, Mar. 2019, doi: https://doi.org/10.1038/s41467-019-09349-w."

[6] M. Imbault, D. Chauvet, J.-L. Gennisson, L. Capelle, and M. Tanter, "*Scientific Reports*, vol. 7, art. 7304, Aug. 2017, doi: https://doi.org/10.1038/s41598-017-06474-8."

[7] C. Rabut, S. L. Norman, W. S. Griggs, J. J. Russin, K. Jann, V. Christopoulos, C. Liu, R. A. Andersen, and M. G. Shapiro, "*Science Translational Medicine*, vol. 16, no. 749, art. eadj3143, May 2024, doi: https://doi.org/10.1126/scitranslmed.adj3143."

[8] D. E. Soulioti, R. M. Jones, and G. F. Pinton, "*Physics in Medicine & Biology*, vol. 70, no. 16, art. 165010, Aug. 2025, doi: https://doi.org/10.1088/1361-6560/adf2f3."

[9] S. Kim, N. Kwon, M. M. Hossain, J. Bendig, and E. E. Konofagou, "*NeuroImage*, vol. 298, art. 120768, Sep. 2024, doi: https://doi.org/10.1016/j.neuroimage.2024.120768."

[10] J. Bendig, C. Aurup, S. G. Blackman, E. P. McCune, S. Kim, and E. E. Konofagou, "*bioRxiv*, Apr. 2025."

[11] J. A. Feshitan, C. C. Chen, J. J. Kwan, and M. A. Borden, "Journal of Colloid and Interface Science, vol. 329, no. 2, pp. 316–324, Jan. 2009, doi: https://doi.org/10.1016/j.jcis.2008.09.066."